Hindawi
Mathematical Problems in Engineering
Volume 2018, Article ID 3723949, 13 pages
https://doi.org/10.1155/2018/3723949

Research Article

Research on the Recognition Algorithm concerning Geometric Boundary regarding Heat Conduction Based on BEM and CGM

Shoubin Wang[1], **Huangchao Jia**[1], **Xiaogang Sun**[2] and **Li Zhang**[1]

[1]*School of Control and Mechanical Engineering, Tianjin Chengjian University, Tianjin 300384, China*
[2]*School of Electrical Engineering and Automation, Harbin Institute of Technology, Harbin 150001, China*

Correspondence should be addressed to Shoubin Wang; wsbin800@126.com

Received 4 April 2018; Revised 5 September 2018; Accepted 9 September 2018; Published 3 October 2018

Academic Editor: Filippo de Monte

An inverse algorithm on boundary element method and conjugate gradient method is proposed to solve the problem of thermal conduction inverse of geometric shape. The direct problem is solved with the boundary element method, while the solution to the inverse problem is obtained through optimizing the objective function in the conjugate gradient method. Taking into account the identification of different material specimens when the unknown boundary is sinusoidal, step function, or circular shape, the influence of initial value, temperature error, thermal conductivity, and thermal intensity on the precision of inversion solution is discussed. The experimental results show that the method can recognize various irregular boundaries and is insensitive to initial values, measurement errors, and heat intensity. The thermal conductivity has a certain effect on this method. The inversion accuracy is higher on the condition that the thermal conductivity is smaller.

1. Introduction

The direct problem [1] of heat conduction is to determine the temperature field in domains, when the boundary condition, thermal performance, heat source, and geometric boundary shape regarding heat conduction are known. Conversely, the inverse problem [2] of heat conduction is to determine the boundary condition [3, 4], heat source [5], thermal performance [6], etc. through measuring the temperature in the domain or on the surface. When the geometric boundary shape of the heat conduction problem is changing or unknown, it needs to use the boundary recognition method to predict the unknown shape, which is a geometric inverse problem of heat conduction.

As a branch of heat transfer inverse problem, thermal geometry inverse problem has a wide range of application prospects in many fields, such as industrial equipment detection, nondestructive testing [7], optimization of geometric shape [8], and biological focus [9]. When the inversion regarding the geometric boundary of the heat conduction system is conducted, the two-dimension steady-state space should be dispersed firstly; the discrete methods mainly include finite difference method [10] (FDM), finite element method [11] (FEM), and boundary element method [12] (BEM), and they can be used to solve the direct problem of heat transfer theory; and the inversion of the geometric boundary can be realized through various optimization technologies based on solving the direct problem. The inversion method based on optimized technology can be divided into the optimized algorithm based on gradient and the optimized algorithm based on nongradient; the optimized algorithm based on gradient mainly includes conjugate gradient method (CGM), Levenberg-Marquardt [13] (L-MM), and steepest descent method (SDM), while the optimized algorithm based on nongradient mainly includes genetic algorithm [14] (GA), neural network algorithm [15] (NNM), and particle swarm algorithm [16] (PSO).

Fan Chunli et al. [17] used FEM to invert internal defects and discussed the influence of initial values and measurement errors on the inversion results. Chen Yi [18] et al. adopted the finite element method to monitor the erosion of the blast furnace bottom. These methods are all calculation methods based on grids. Because the shape of the solution domain varies, it needs to repeatedly divide the complex grids or units

regarding the solution domain. Thus the solution process becomes extremely complex, and the calculation quantity is very large. This problem can be well avoided through BEM, the control equation of the described problem is transformed to the boundary integral equation only related to the boundary. The dimension of the problem is reduced by 1, and it does not need to scatter the interior domain. It only needs to scatter the boundary, and the shape of the unknown boundary can be easily modified. The complex reset calculation of grids is successfully avoided, and it also overcomes the difficulty caused by the distortion of grids or units in the geometric inversion process. From the aspect of geometric inversion problem, the boundary element method has obvious advantages compared with other value methods.

There are many optimization algorithms in solving the inverse problem of heat conduction geometry. Fan Chunli et al. [19, 20] indicated that L-M method was very effective when there were few recognition parameters. Huang et al. [21] compared the L-M method with the CGM used for the geometric inversion problem of heat conduction, and the research indicated that CGM was more effective than the L-M method. This advantage was more obvious when there were many recognition parameters. It was mainly embodied in the following: (1) the calculation time was very short; (2) no exact initial value was required; (3) less measurement points were required. The optimized algorithm of CGM was adopted in the paper based on above literature study.

In actual engineering application, the shape of the unknown boundary is mostly irregular. In order to improve the application range of boundary recognition, it is very important to study the boundary recognition of irregular shape. The BEM and CGM were combined in the paper, and they were used to solve the recognition problem regarding irregular geometric boundary shapes. The recognition of test pieces concerning different materials in the shapes such as sine wave, step function, and round on the unknown boundary was considered, and the influence of factors such as initial value, temperature measurement error, thermal conductivity, and heating intensity on the precision of inverse solution was discussed.

2. Direct Problem of Heat Conduction Based on BEM

2.1. Overview and Features of BEM. Boundary Element Method (BEM) is a calculation method developed on the basis of classical integral equation, which absorbs the discretization technology of finite element method. The basic principle of BEM is to solve the calculus equation in the method regarding the integral equation. After the first international conference of BEM in 1978, it was greatly applied and developed, and it was widely applied to many fields [22–24] such as elastic mechanics, fluid mechanics, rock mechanics, and heat transfer theory.

The foundation of BEM is to establish the integral equation, and the solution process can be divided into the following two steps.

The first step is to demarcate the problem and apply Green formula to transform the differential equation in the solution domain into the integral equation on the boundary by fundamental solution.

In this way, the dimensionality of the equation solution problem is reduced by one dimension; for example, the three-dimensional space problem is reduced to a two-dimensional plane problem, and the two-dimensional plane problem is reduced to a one-dimensional problem. So the input data quantity and the unknown quantity of the algebraic equation set are greatly reduced, and this is significant feature of BEM compared with the FEM.

The second step is the discretization of the boundary, which can use the discretization technique of finite element method. Moreover, since the discretization is only conducted on the boundary and error only exists on the boundary, while the unknown quantity in the domain can be calculated through the analytical equation, so the calculation precision can be higher. In addition, because of the singularity regarding the basic solution, the BEM has high precision in solving the singular problem. In conclusion, the BEM has outstanding advantages, such as reducing dimensionality, less input data, high calculation precision, especially suitable for large area, and singular problems.

The solution to the direct problem regarding the heat conduction is the basis and premise to realize the inverse problem of heat transfer theory. When the geometric inverse problem of heat transfer theory is solved, the solution to the direct problem of the heat conduction is very complex because the geometric boundary shape is uncertain. At present in the geometric inverse problem of heat transfer theory, the boundary element method (BEM) and the finite element method (FEM) are two main methods to solve the direct problems. BEM is a developed calculation method based on the classic integral equation, and it absorbs the discrete technology of the value methods such as FEM; the basic thought is to solve the calculus equation with the method of the integral equation. Compared with FEM, the solution to the direct problem regarding the heat conduction with BEM has the following features [25]:

(1) BEM only needs to discretize the system on the boundary, which avoids the disadvantage that FEM needs to remesh the whole solution area every iteration and obviously reduces the computational dimension and workload.

(2) Because the basic solution adopted by BEM is applicable to infinite or semi-infinite domain, it is not necessary to determine the outer boundary when solving the problem in infinite or semi-infinite domain; thus the problem is greatly simplified.

(3) The solution error of the BEM is only generated on the boundary. The value of function and coefficient in the domain can be obtained by analytic formula; thus the error source is few and calculation precision is high.

(4) BEM fundamental solution itself is derivable and can be used to solve singularity problems.

In the process of solving inverse heat transfer geometric problems, the objective function needs to be optimized continuously. Because of the change of the shape of the solution area, the finite difference method and the finite element method need to redivide the solution area into complicated meshes or elements in each iteration, which increases the difficulty and computational complexity of solving the direct

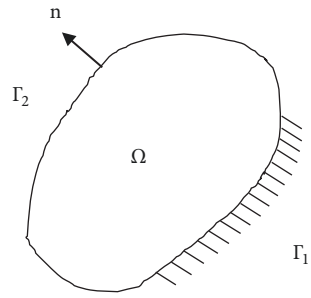

Figure 1: Boundary Γ_1 and Γ_2.

problem. It only needs to conduct discretization regarding the system on the boundary for BEM; thus it avoids the shortcoming of repeatedly dividing grids in the overall solution domain in all iterations for FEM; it also obviously reduces calculation dimensionality, solution difficulty, and calculation quantity of the direct problems for BEM.

2.2. Boundary Integral Equation. As shown in Figure 1, the boundary integral equation is deducted in the weighted residual method; because many projects can be described in the forms of Laplace's equation, the definite solution problem of the Laplace's equation is considered, namely. Boundary Γ_1 and Γ_2 are shown in Figure 1.

In the domain Ω,

$$\nabla^2 u = 0 \tag{1}$$

On the boundary Γ_1,

$$u = \overline{u} \tag{2}$$

On the boundary Γ_2,

$$q = \frac{\partial u}{\partial n} = \overline{q} \tag{3}$$

Its expression of the weighted residual is

$$\int_\Omega \left(\nabla^2 u\right) W d_\Omega = \int_{\Gamma_2} \left(q - \overline{q}\right) W d_\Gamma - \int_{\Gamma_2} \left(u - \overline{u}\right) \frac{\partial W}{\partial n} d_\Gamma \tag{4}$$

Take the weighted function W as the basic solution u^*, and then correspondingly

$$\int_\Omega \left(\nabla^2 u\right) u^* d\Omega = \int_{\Gamma_2} \left(q - \overline{q}\right) u^* d\Gamma - \int_{\Gamma_1} \left(u - \overline{u}\right) q^* d\Gamma \tag{5}$$

Integration by parts is conducted regarding the Laplace operator, and Green Equation is applied, then

$$\int_\Omega \left(\frac{\partial P}{\partial x} + \frac{\partial \Omega}{\partial y}\right) d_\Omega = \int_\Gamma \left(P d_y + Q d_x\right) \tag{6}$$

So the left item of (5) is

$$\begin{aligned} \int_\Omega \left(\nabla^2 u\right) u^* d_\Omega &= \int_\Omega \nabla\left(u^* \nabla u\right) d_\Omega - \int_\Omega \nabla u \left(\nabla u^*\right) d_\Omega \\ &= \int_\Gamma \left(\nabla u\right) u^* d_\Gamma - \int_\Omega \left(\nabla u\right)\left(\nabla u^*\right) d_\Omega \\ &= \int_\Gamma \frac{\partial u}{\partial n} u^* d_\Gamma - \int_\Omega \left(\nabla u\right)\left(\nabla u^*\right) d_\Omega \end{aligned} \tag{7}$$

Integration by part and Green Equation are applied to the second item on the right of (7),

$$\begin{aligned} \int_\Omega \left(\nabla u\right)\left(\nabla u^*\right) d_\Omega &= \int_\Omega \nabla\left(u \nabla u^*\right) d_\Omega \\ &\quad - \int_\Omega u\left(\nabla^2 u^*\right) d_\Omega \\ &= \int_\Gamma u \cdot \frac{\partial u^*}{\partial n} d_\Gamma - \int_\Omega u \cdot \nabla^2 u^* d_\Omega \end{aligned} \tag{8}$$

So, there is

$$\begin{aligned} \int_\Omega \left(\nabla^2 u\right) u^* d_\Omega &= \int_\Gamma \frac{\partial u}{\partial n} u^* d_\Gamma - \int_\Gamma u \cdot \frac{\partial u^*}{\partial n} d_\Gamma \\ &\quad + \int_\Omega u \cdot \nabla^2 u^* d_\Omega \end{aligned} \tag{9}$$

Substitute it into (5); because $\Gamma = \Gamma_1 + \Gamma_2 + \Gamma_3$ and $q = \partial u/\partial n$, $q^* = \partial u^*/\partial n$, so

$$\begin{aligned} \int_\Omega \left(\nabla^2 u^*\right) u d_\Omega &= \int_{\Gamma_1} \overline{u} q^* d_\Gamma + \int_{\Gamma_2} u q^* d_\Gamma - \int_{\Gamma_1} q u^* d_\Gamma \\ &\quad - \int_{\Gamma_2} \overline{q} u^* d_\Gamma \end{aligned} \tag{10}$$

The first, second, third, and fourth item on the right can be, respectively, combined together, namely.

$$\int_\Omega \left(\nabla^2 u^*\right) u d_\Omega = \int_\Gamma u q^* d_\Gamma - \int_\Gamma q u^* d_\Gamma \tag{11}$$

Weighted function $u*$ is the basic solution of the Laplace's equation, and it satisfies

$$\nabla^2 u^* + \delta\left(r - r_1\right) = 0 \tag{12}$$

In the equation, the point "i" indicates the focus point of the unit point source, so

$$\nabla^2 u^* = -\delta\left(r - r_1\right) \tag{13}$$

Substitute it into (10) or (11), and there is

$$u_i + \int_{\Gamma_1} q u^* d_\Gamma + \int_{\Gamma_2} \overline{q} u^* d_\Gamma = \int_{\Gamma_1} \overline{u} q^* d_\Gamma + \int_{\Gamma_2} u q^* d_\Gamma \tag{14}$$

$$u_i + \int_\Gamma u q^* d_\Gamma = \int_\Gamma q u^* d_\Gamma \tag{15}$$

Equations (14) and (15) are effective regarding all points in the domain Ω, and they are called the integral function of internal node. It indicates that the function value u_i regarding all points in domain Ω can be indicated with the integral of u and its normal derivative q on the boundary; if all values of u and q on the boundary are obtained, u and q regarding all internal points can be calculated through (15).

It needs to transfer the point i to the boundary so as to obtain the integral equation regarding all points on the boundary, but the singularity of the integral $\partial u^*/\partial n$ shall

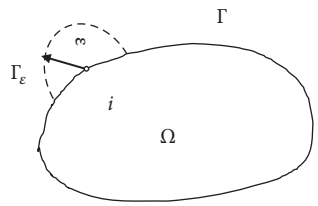

Figure 2: Boundary point surrounded by the hemisphere.

be considered; the boundary near the point i is substituted by the hemisphere in radius ε to avoid that point i becomes singularity point; then the hemisphere ε tends to 0, so point i becomes the boundary point. Boundary point surrounded by the hemisphere is shown in Figure 2.

Without loss of generality, suppose the boundary belongs to Γ_2 type, the point i is an internal point, and then (15) can be

$$\begin{aligned} &u_i + \int_{\Gamma_{(2-\varepsilon)}} uq^* d_\Gamma + \int_{\Gamma_\varepsilon} uq^* d_\Gamma \\ &\quad = \int_{\Gamma_{(2-\varepsilon)}} qu^* d_\Gamma + \int_{\Gamma_\varepsilon} qu^* d_\Gamma \end{aligned} \tag{16}$$

$$\int_{\Gamma_\varepsilon} uq^* d_\Gamma = \int_{\Gamma_\varepsilon} u \frac{\partial (1/4\pi r)}{\partial n} d_\Gamma = -\int_{\Gamma_\varepsilon} u \frac{1}{4\pi\varepsilon^2} d_\Gamma \tag{17}$$

Suppose the boundary is smooth, it can be obtained through the mean value theorem of integrals that

$$\int_{\Gamma_\varepsilon} uq^* d_\Gamma = -\int_{\Gamma_\varepsilon} u \frac{1}{4\pi\varepsilon^2} d_\Gamma = u(\xi) \frac{-1}{4\pi\varepsilon^2} 2\pi\varepsilon^2 \tag{18}$$

where ξ is a point in Γ_ε.

Suppose $\varepsilon \longrightarrow 0$ and $u(\xi) \longrightarrow u_i$, then

$$\lim_{\varepsilon \longrightarrow 0} \left(\int_{\Gamma_\varepsilon} uq^* d_\Gamma \right) = -\frac{1}{2} u^i \tag{19}$$

Equation (19) is also applicable to smooth two-dimension boundary; similarly

$$\begin{aligned} \lim_{\varepsilon \longrightarrow 0} \left(\int_{\Gamma_\varepsilon} qu^* d_\Gamma \right) &= \lim_{\varepsilon \longrightarrow 0} \left(\int_{\Gamma_\varepsilon} \frac{1}{4\pi\varepsilon} q d_\Gamma \right) \\ &= \lim_{\varepsilon \longrightarrow 0} \frac{1}{4\pi\varepsilon} q(\xi) 2\pi\varepsilon^2 \\ &= \lim_{\varepsilon \longrightarrow 0} \frac{1}{2} q(\xi) \varepsilon = 0 \end{aligned} \tag{20}$$

$$\lim_{\varepsilon \longrightarrow 0} \left(\int_{\Gamma_{(2-\varepsilon)}} uq^* d_\Gamma \right) = \int_{\Gamma_2} uq^* d_\Gamma \tag{21}$$

$$\lim_{\varepsilon \longrightarrow 0} \left(\int_{\Gamma_{(2-\varepsilon)}} qu^* d_\Gamma \right) = \int_{\Gamma_2} qu^* d_\Gamma \tag{22}$$

When point i is in the Γ_1, the same result will be obtained, so

$$\frac{1}{2} u^i + \int_\Gamma uq^* d_\Gamma = \int_\Gamma qu^* d_\Gamma \tag{23}$$

This is the boundary integral equation of Laplace's equation.

The integral equation (15) of the internal node point and the boundary integral equation (23) regarding the boundary node point are combined, then

$$C_i u_i + \int_\Gamma uq^* d_\Gamma = \int_\Gamma qu^* d_\Gamma \tag{24}$$

When $i \in \Omega$, $C_i = 1$; when $i \in \Gamma$ (smooth boundary), $C_i = 1/2$.

2.3. Discretion of the Boundary Integral Equation. Formula (24) is discretized and the boundary is divided into N units, the constant element, linear element, or secondary element can be adopted to conduct uniform interpolation regarding u and q, and then the matrix is formed according to different interpolations regarding all boundary elements:

$$\sum_{j=1}^{N} H_{ij} T_j = \sum_{j=1}^{N} G_{ij} q_j \tag{25}$$

Namely,

$$HT = Gq \tag{26}$$

$H_{ii} = C_i + \widehat{H}_{ii}$ (when $i = j$) and $H_{ij} = \widehat{H}_{ij}$ (when $i \neq j$); the unknown quantity is transferred to the right, and the known quantity is transferred to the left, then

$$AX = F \tag{27}$$

The unknown quantity in u and q can be obtained by solving above equation set.

2.4. Calculation Example regarding Direct Problems concerning Heat Conduction Based on BEM. The two-dimension steady-state model [24] of heat conduction without thermal internal source for internal surface flaw detection concerning industrial equipment is shown in Figure 3. The domain Ω is a two-dimension space composed of x = 0.0, x = 10.0, y = 0, and y = f(x). It is adiabatic on both sides of x = 0.0 and x = 10.0, and a known constant heat flux q_0 flows at y = 0 through cooling; thus a constant known temperature T_0 is maintained for y = f(x).

The temperature distribution Y_i at y = 0 can be measured through the infrared scanning thermal-detector, and it aims to detect the fault in internal surface regarding industrial thermal equipment through back-stepping the shape f(x) of the internal surface flaw; the mathematical model is as follows:

The heat conduction equation in domain Ω is

$$\frac{\partial^2 T}{\partial x^2} + \frac{\partial^2 T}{\partial y^2} = 0 \tag{28a}$$

When $x = 0$ and $x = 10$, the heat conduction equation is

$$\frac{\partial T}{\partial x} = 0 \tag{28b}$$

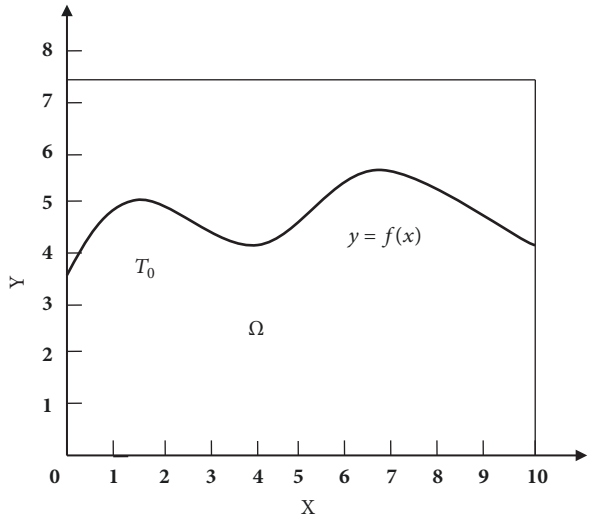

FIGURE 3: Physical model of internal surface flaw detection for thermal equipment.

When $y = 0$, the heat conduction equation is

$$-\frac{\partial T}{\partial y} = q_0 \tag{28c}$$

When $y = f(x)$, the heat conduction equation is

$$T = T_0 \tag{28d}$$

$$T(x_i, 0) = Y_i \quad (i = 1, 2, \cdots, m) \tag{28e}$$

According to the boundary integral equation in Section 2.2 and its discretion knowledge in Section 2.3, the unknown temperature and heat flux on the boundary can be obtained. Boundary temperature and heat flux obtained from boundary element are shown in Figure 4. Temperature of internal points through BEM is shown in Figure 5.

3. CGM Algorithm regarding the Geometric Inverse Problem concerning Heat Transfer Theory

3.1. The Principle of the CGM. The solution to the inverse problems can be transformed to the following optimization control problem concerning functional variation mathematically:

$$J(f(x)) = \|T_i - Y_i\|^2 = \sum_{i=1}^{m} [T_i(x, 0) - Y_i(x, 0)]^2 \tag{29}$$

$Y_i(x, 0)$ is the actual measured temperature value regarding the measurement point on the model surface; $T_i(x, 0)$ is the calculated temperature value concerning the measurement point from above equation set based on the guessed boundary shape.

The iterative solution method is used to search the standard problem regarding boundary shape $f(x)$ involved with iteration stop, and it is related to the error of temperature measurement. If there is no measurement error, the stop standard is

$$J\left[f^{k+1}(x)\right] < \varepsilon \tag{30}$$

ε is a minor number such as 0.01, and it should be determined based on the specific convergence. If there is a measurement error and the standard deviation of the temperature measurement is σ, the lowest standard can be determined based on the error principle

$$\varepsilon = 3\sigma \tag{31}$$

The conjugate gradient [26] transforms the inverse problem to three problems: direct problem, sensitivity problem, and adjoint problem. The direct problem is based on the assumed boundary shape equations (28a), (28b), (28c), (28d), and (28e) and other boundary conditions; then the equations of boundary conditions are solved through BEM, and the minimum of the objective function (29) is calculated. The cyclic way of the CGM is

$$f^{n+1}(x) = f^n(x) - \beta^n p^n(x) \quad n = 0, 1, 2 \cdots \tag{32}$$

β^n is the step size in search from the nth to the (n+1)th iteration; $p^n(x)$ is the search direction; namely,

$$p^n(x) = J'^n(x) + \gamma^n p^{n-1}(x) \tag{33}$$

$J'^n(x)$ is the gradient direction, so the nth search direction $p^n(x)$ is the conjugate between the gradient direction $J'^n(x)$ and the (n-1)th search direction $p^{n-1}(x)$; γ^n is the conjugate coefficient, and it can be calculated as follows:

$$\gamma^n = \frac{\int_{x=0}^{L} \left(J'^n\right)^2 d_x}{\int_{x=0}^{L} \left(J'^n - 1\right)^2 d_x} \tag{34}$$

$\gamma^0 = 0$.

3.2. Sensitivity Problem. To confirm the step size β^n in search of (32), a so-called sensitivity problem, namely, the increment problem needs to be solved. The sensitivity problem refers to the variation $\Delta T(x)$ of surface temperature T, when the boundary shape $f(x)$ has an increment $\Delta f(x)$.

$$\left(\frac{\partial J}{\partial f}\right)^T = \left(\frac{\partial J}{\partial f_1}, \frac{\partial J}{\partial f_2}, \cdots, \frac{\partial J}{\partial f_n}\right) \tag{35}$$

The specific way is in (29), and the original T is replaced by $T + \Delta T$, while the original $f(x)$ is replaced by $f(x) + \Delta f(x)$; then the sensitivity problem is obtained by subtracting the original equations; namely,

The heat conduction problem is as follows in the domain Ω:

$$\frac{\partial^2 \Delta T}{\partial x^2} + \frac{\partial^2 \Delta T}{\partial y^2} = 0 \tag{36a}$$

X	Y	Temperature	Heat Flux
2.500000e- 001	0.000000e+000	6.390025e+001	-2.000000e+001
7.500000e- 001	0.000000e+000	6.321133e+001	-2.000000e+001
1.250000e+000	0.000000e+000	6.239535e+001	-2.000000e+001
1.750000e+000	0.000000e+000	6.176625e+001	-2.000000e+001
2.250000e+000	0.000000e+000	6.157829e+001	-2.000000e+001
2.750000e+000	0.000000e+000	6.197711e+001	-2.000000e+001
3.250000e+000	0.000000e+000	6.303188e+001	-2.000000e+001
3.750000e+000	0.000000e+000	6.475691e+001	-2.000000e+001
4.250000e+000	0.000000e+000	6.711852e+001	-2.000000e+001
4.750000e+000	0.000000e+000	7.002989e+001	-2.000000e+001
5.250000e+000	0.000000e+000	7.333570e+001	-2.000000e+001
5.750000e+000	0.000000e+000	7.678936e+001	-2.000000e+001
6.250000e+000	0.000000e+000	8.003339e+001	-2.000000e+001
6.750000e+000	0.000000e+000	8.261087e+001	-2.000000e+001
7.250000e+000	0.000000e+000	8.405156e+001	-2.000000e+001
7.750000e+000	0.000000e+000	8.404103e+001	-2.000000e+001
8.250000e+000	0.000000e+000	8.257417e+001	-2.000000e+001
8.750000e+000	0.000000e+000	7.996230e+001	-2.000000e+001
9.250000e+000	0.000000e+000	7.671788e+001	-2.000000e+001
9.750000e+000	0.000000e+000	7.326159e+001	-2.000000e+001
1.000000e+001	7.500000e- 002	7.317781e+001	-2.000000e+001

Figure 4: Boundary temperature and heat flux obtained from boundary element.

X	Y	Temperature
2.000000e+000	1.000000e+000	8.050599e+001
4.000000e+000	5.000000e- 001	7.557470e+001
6.000000e+000	5.000000e- 001	8.867413e+001
8.000000e+000	5.000000e- 001	9.415732e+001
1.000000e+001	1.000000e+000	4.513013e+001

Figure 5: Temperature of internal points through BEM.

The heat conduction problem is as follows when $x = 0$:

$$\frac{\partial \Delta T}{\partial x} = 0 \tag{36b}$$

The heat conduction problem is as follows when $x = 10$:

$$\frac{\partial \Delta T}{\partial x} = 0 \tag{36c}$$

The heat conduction problem is as follows when $y = 0$:

$$\frac{\partial \Delta T}{\partial y} = 0 \tag{36d}$$

The heat conduction problem is as follows when $y = f(x)$:

$$\Delta T = \Delta f \frac{\partial T}{\partial y} \tag{36e}$$

The above equation set can be solved by discretization through BEM similarly, and the temperature increment ΔT can be obtained. $J(f^{n+1})$ can be as follows regarding the (n+1)th iteration according to (29)

$$J\left(f^{n+1}\right) = \sum_{i=1}^{m} \left[T_i\left(f^n - \beta^n p^n\right) - Y_i\right]^2 \tag{37}$$

Conduct Taylor expansion regarding $T_i(f^n - \beta^n p^n)$ to remove 2 linear items to obtain

$$J\left(f^{n+1}\right) = \sum_{i=1}^{m} \left[T_i\left(f^n\right) - \beta^n \Delta T_i\left(p^n\right) - Y_i\right]^2 \tag{38}$$

Derive and set β^n at 0, and then the step size Γ in search can be obtained; namely,

$$\beta^n = \frac{\sum_{i=1}^{m} \left(T_i - Y_i\right)^2 \Delta T_i}{\sum_{i=1}^{m} \left(\Delta T_i\right)^2} \tag{39}$$

3.3. Adjoint Problem. The new boundary shape function $f^{n+1}(x)$ can be calculated according to the boundary shape function $f^n(x)$ of last iteration in (32), and the search direction $p^n(x)$ can also be obtained; so the gradient direction

$J'^{n}(x)$ should be solved according to (33), namely, the so-called functional derivation problem, and it is also called adjoint problem. To derive the equation in the adjoint direction, the basic control equation (28a) is multiplied by a Lagrange operator $\lambda(x, y)$ (also called adjoint function); then integration is applied to the spatial domain, and the result is added to the right of (29); thus the expression of the functional $J[f(x)]$ can be obtained.

$$J[f(x)] = \int_{x=0}^{L} [T-Y]^2 \delta(x-x_i)\, d_x + \int_{x=0}^{L}\int_{y=0}^{f(x)} \lambda\left[\frac{\partial^2 T}{\partial x^2} + \frac{\partial^2 T}{\partial y^2}\right] d_y\, d_x \tag{40}$$

Substitute T with $T + \Delta T$ and substitute f with $f + \Delta f$, and it is obtained through a series of transformation that

$$\int_a^b [T-Y]^2 d_x = \int_a^b \int_0^L [T-Y]^2 \delta(x-x_i)\, d_x\, d_y \tag{41}$$

Then

$$\begin{aligned}\Delta J &= \Delta J(q+\Delta q) - J(q) \\ &= \int_{x=0}^{L} 2[T-Y]\delta(x-x_i)\, d_x \\ &= \int_{x=0}^{L}\int_{y=0}^{f(x)} \lambda\left[\frac{\partial^2 \Delta T}{\partial x^2} + \frac{\partial^2 \Delta T}{\partial y^2}\right]_i d_y\, d_x\end{aligned} \tag{42}$$

The integration by parts is conducted regarding the second item on the right of (42) twice, and then the boundary condition of the sensitivity problem is used and then makes ΔJ tend to 0 to obtain the adjoint problem.

In the domain Ω,

$$\frac{\partial^2 \lambda}{\partial x^2} + \frac{\partial^2 \lambda}{\partial y^2} = 0 \tag{43a}$$

When $x = 0$,

$$\frac{\partial \lambda}{\partial x} = 0 \tag{43b}$$

When $x = 10$,

$$\frac{\partial \lambda}{\partial y} = 0 \tag{43c}$$

When $y = 0$,

$$\frac{\partial \lambda}{\partial y} = -2(T-Y)\delta(x-x_i) \tag{43d}$$

When $y = f(x)$,

$$\lambda = 0 \tag{43e}$$

The corresponding value of the adjoint function $\lambda(x, y)$ is obtained through the BEM, and then the functional increment is

$$\Delta J = \int_0^L -\left[\frac{\partial \lambda}{\partial y}\cdot\frac{\partial T}{\partial y}\right]_{y=f(x)} \Delta f(x)\, d_x \tag{44}$$

So there is the following equation according to the definition of Alifanov

$$\Delta J = \int_0^L J'(x)\, \Delta f(x)\, d_x \tag{45}$$

The derivative of the functional J is

$$J'(x) = \left(-\frac{\partial \lambda}{\partial y}\cdot\frac{\partial T}{\partial y}\right)_{y=f(x)} \tag{46}$$

Above three problems including direct problem, sensitivity problem and adjoint problem are solved, then the iterative calculation steps of CGM can be given.

(1) Select a guessed initial value $f(x)$ of internal surface shape to solve direct problems (28a), (28b), (28c), (28d), and (28e) and calculate the temperature distribution $T(x, t)$ in the domain.

(2) Judge whether it satisfies the standard equation $J[f^{k+1}(x)] < \varepsilon$ of convergence stop according to T_i and Y_i; if it satisfies, stop the iteration or calculate based on the next step.

(3) Solve the adjoint problem equations (43a), (43b), (43c), (43d), and (43e) to obtain the adjoint function $\lambda(x)$.

(4) Calculate the gradient $J'(x)$.

(5) Calculate the coefficient γ^k and the descent direction p^k of the conjugate gradient.

(6) Suppose $\Delta f(x) = -p^k(x)$, solve the sensitivity problem equations (36a), (36b), (36c), (36d), and (36e) to obtain the temperature increment $\Delta T(x)$.

(7) Calculate the step size β^k in search based on (39).

(8) Suppose $k = k+1$ and obtain the new boundary shape $f^k(x)$; the new T_i returns to the 2nd step.

4. Simulation Result of the Internal Surface Shape Recognition

To verify the effectiveness of the internal boundary shape through CGM, the two boundaries in shapes of sine curve (example A) step function curve (example B) are, respectively, researched. The outside diameter of pipe in-wall is 0.18 m; surface coefficient regarding heat transfer of the internal surface is 1000 W/(m^2·K); surface coefficient regarding heat transfer of the external surface is 10 W/(m^2·K). Two kinds of materials are adopted for the pipe: one is chromium-nickel steel regarding thermal conductivity 15.2 W/(m^2·K); the other is cement concerning thermal conductivity 0.5 W/(m^2·K). The corresponding examples to the two materials are respectively marked as A(1), B(1) and A(2), B(2).

4.1. Recognition Result of Different Initial Boundary Hypothesis. Figures 6 and 7 are the identification results of the boundary shapes of the inner wall of examples A and B under different initial boundary assumptions. Influence of the initial boundary hypothesis on the recognition result of in-wall boundary A ($\varepsilon = 1.0$) is shown in Figure 6. Influence of the initial boundary hypothesis on the recognition result of in-wall boundary B ($\varepsilon = 1.0$) is shown in Figure 7.

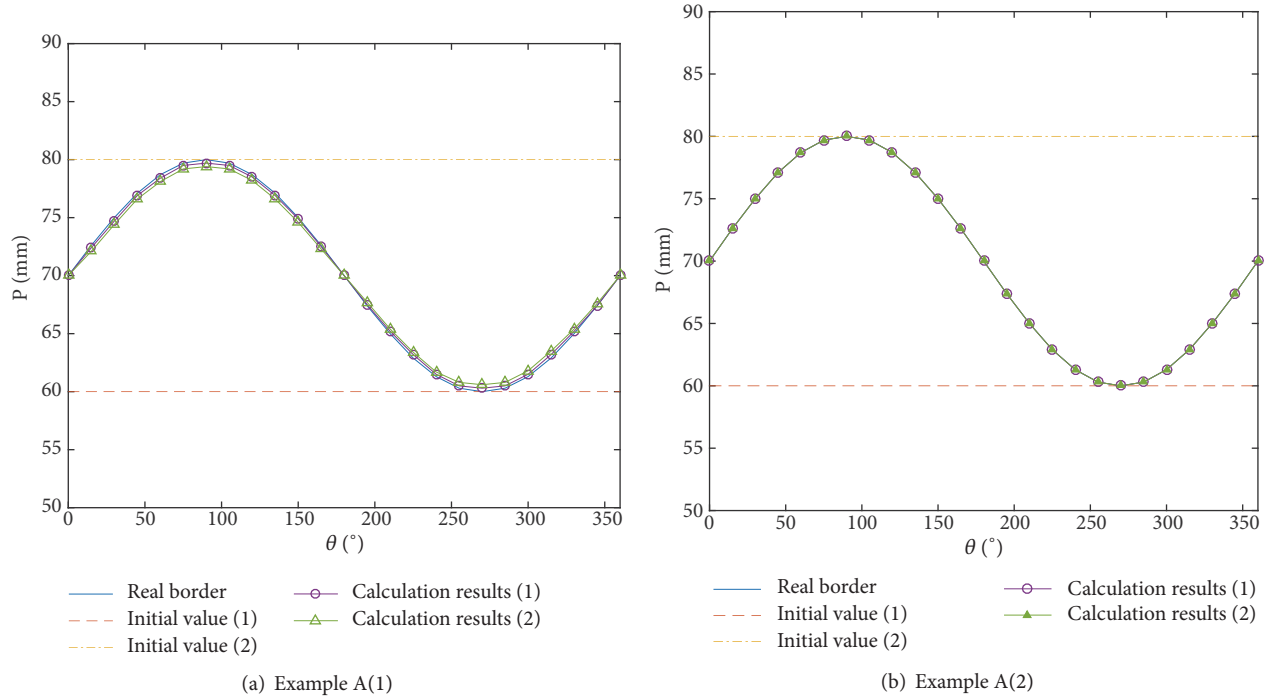

(a) Example A(1) (b) Example A(2)

Figure 6: Influence of the initial boundary hypothesis on the recognition result of in-wall boundary A ($\varepsilon = 1.0$).

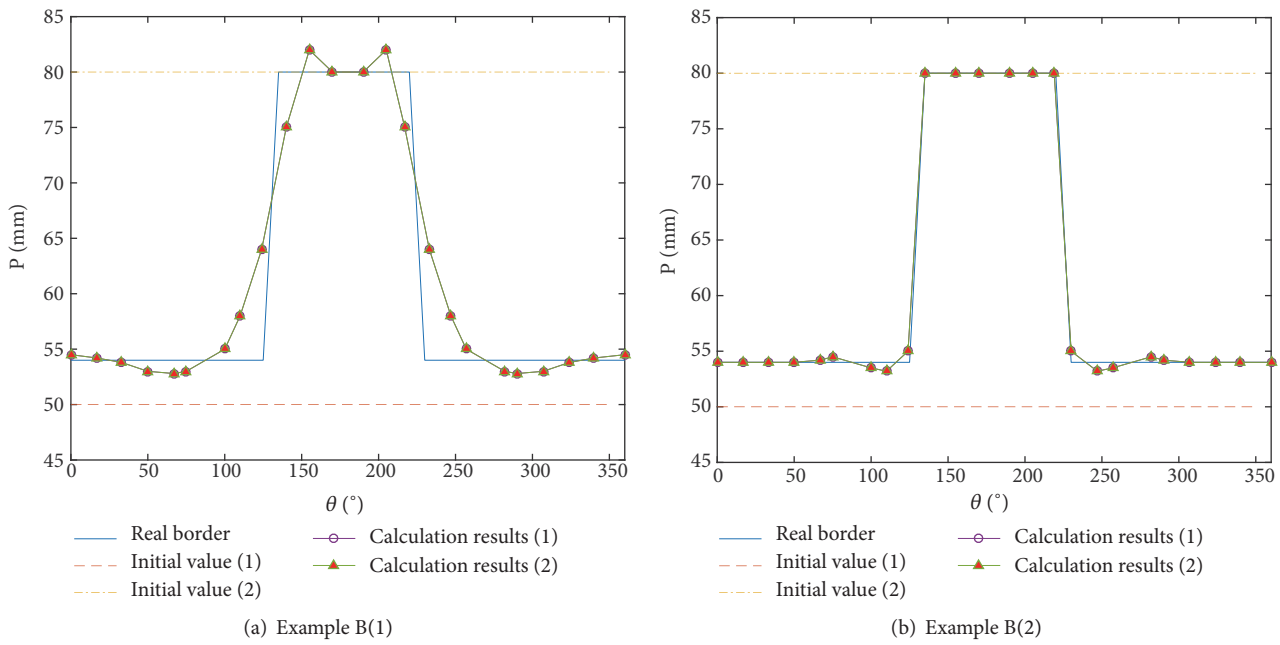

(a) Example B(1) (b) Example B(2)

Figure 7: Influence of the initial boundary hypothesis on the recognition result of in-wall boundary B ($\varepsilon = 1.0$).

The average relative error of the recognition result for different initial values (the internal round boundary of different radiuses is the initial boundary hypothesis) is shown in Table 1. The iterative convergent condition is $\varepsilon = 1.0$.

It can be found from the recognition result of Figures 6 and 7 and Table 1 that the boundary shape of pipe in-wall can be precisely recognized through CGM, and the initial boundary hypothesis has little influence on the recognition result. It can be found that the recognition precision is low if the thermal conductivity is large, when the recognition result regarding the thermal conductivity of different pipes is compared. It is mainly because the thermal resistance is small

Table 1: Average relative error of recognition result under the condition of different initial values.

Initial number	Initial value/mm	Average relative error/%		Initial value	Average relative error/%	
		A (1)	A (2)		B (1)	B (2)
1	60	0.8	0.07	50	3.8	0.8
2	80	0.9	0.05	80	3.8	0.8

Table 2: Average relative error of recognition results concerning different temperature measurement errors.

σ/°C	Average relative error/%			
	A (1)	A (2)	B (1)	B (2)
0.5	3.4	0.4	6.2	1.4
1.0	7.2	0.7	9.8	2.1

when the thermal conductivity of pipes is large. Therefore the temperature variation is small upon changing the same pipeline wall thickness.

4.2. Recognition Result of Different Temperature Measurement Errors. Influence of temperature measurement error on the recognition result regarding the in-wall boundary A is shown in Figure 8. Influence of temperature measurement error on the recognition result concerning the in-wall boundary B is shown in Figure 9. The average relative error of recognition results concerning different temperature measurement errors is shown in Table 2.

It can be found that the temperature measurement error has little influence on the recognition result regarding pipeline of small thermal conductivity [example A (2) and example B (2)], when the recognition results of different thermal conductivity are compared on the basis of Figures 8 and 9 and Table 2. The error of the recognition result is large, when the thermal conductivity is high [example A (1) and example B (1)].

The results show that CGM can identify the inner wall shape of pipeline successfully according to the temperature distribution of the testing surface. The initial boundary hypothesis has little influence on the recognition result. The measurement error has certain influence on the final recognition result, and the recognition precision is lower if the measurement error is larger. The adopted boundary condition in the detection process should be changed to obtain precise recognition result. The maximum temperature difference regarding the detection surface should be increased as much as possible, and then the influence of errors on the recognition precision can be reduced.

5. Recognition of Thermal Internal Flaw Shape through CGM

The schematic diagram of the test piece with the heat-type defect studied in this section is shown in Figure 10. The inside of the test piece is steady-state heat transfer, and the temperature at the junction of the defect and the test piece is the same, and the heat flow is equal.

Heat convection is conducted between the outside surface of the test piece and air, and the surface coefficient of heat transfer is 10 W/(m^2·K). Two kinds of materials are adopted in this section concerning the round test piece for comparison research: the heat transfer coefficient of test piece A is 52 W/(m^2·K); the heat transfer coefficient of test piece B is 0.34 W/(m^2·K). The external diameter of the test piece is 0.04 mm. The flaw emits heat evenly, and the thermal power is q_v. The external environmental temperature T_a is 25°C.

5.1. Influence of the Thermal Conductivity regarding the Test Piece and Flaw on the Recognition Result. The recognition result of the internal round flaws for two test pieces at different initial values is shown in Figure 11. When the heat liberation rate q_v of the unit area is 1×10^3 kW/m^2 and the thermal conductivity of flaws is 0.34 W/(m·k).

It can be found from the figure that the shape of this internal flaw can be precisely recognized, and the average error is all 0.24%. The influence of initial values on the recognition result can be ignored.

Recognition result concerning flaw boundary shapes regarding two test pieces at the same initial value is shown in Figure 12. The iterative convergent condition is $\varepsilon = 2.0$.

It can be found from the figure that, for specimen B with small thermal conductivity, the accuracy of boundary shape recognition is higher, and the average relative error is 2.4%. While the recognition result precision of boundary shape is relatively low for the test piece A with large thermal conductivity, and the average relative error is 40%. The main reason is that the difference of thermal conductivity makes the temperature distribution of the same shape defect on the outer surface quite different.

5.2. Influence of Estimated Error regarding Thermal Intensity and Error concerning Temperature Measurement on the Recognition Result. The intensity of heat source is a known condition for the identification and calculation of defect boundary. It can be calculated according to the measurement results of surface temperature and the correlation of natural convection heat transfer of ambient temperature through the surface.

Influence of the calculation error regarding thermal intensity on the recognition result flaws ($\varepsilon = 2.0$) is shown in Figure 13. Influence of random temperature measurement error on the recognition result regarding flaws is shown in

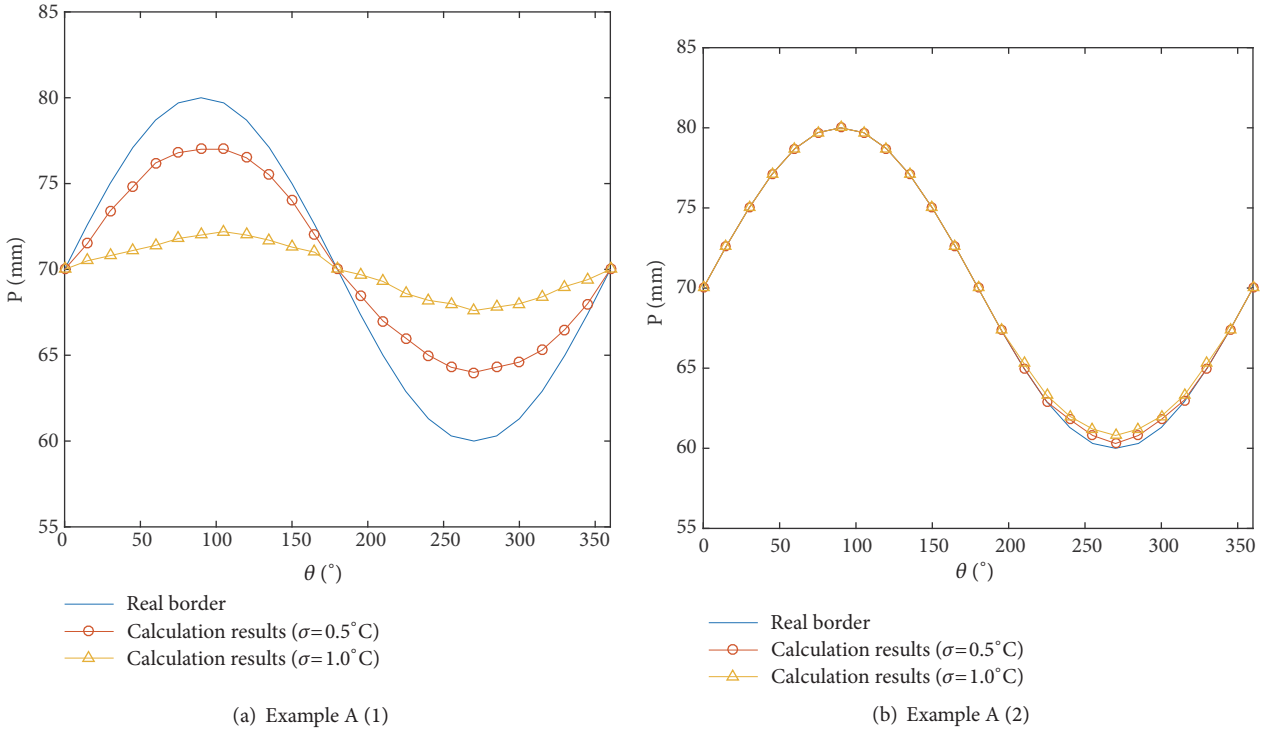

Figure 8: Influence of temperature measurement error on the recognition result regarding the in-wall boundary A.

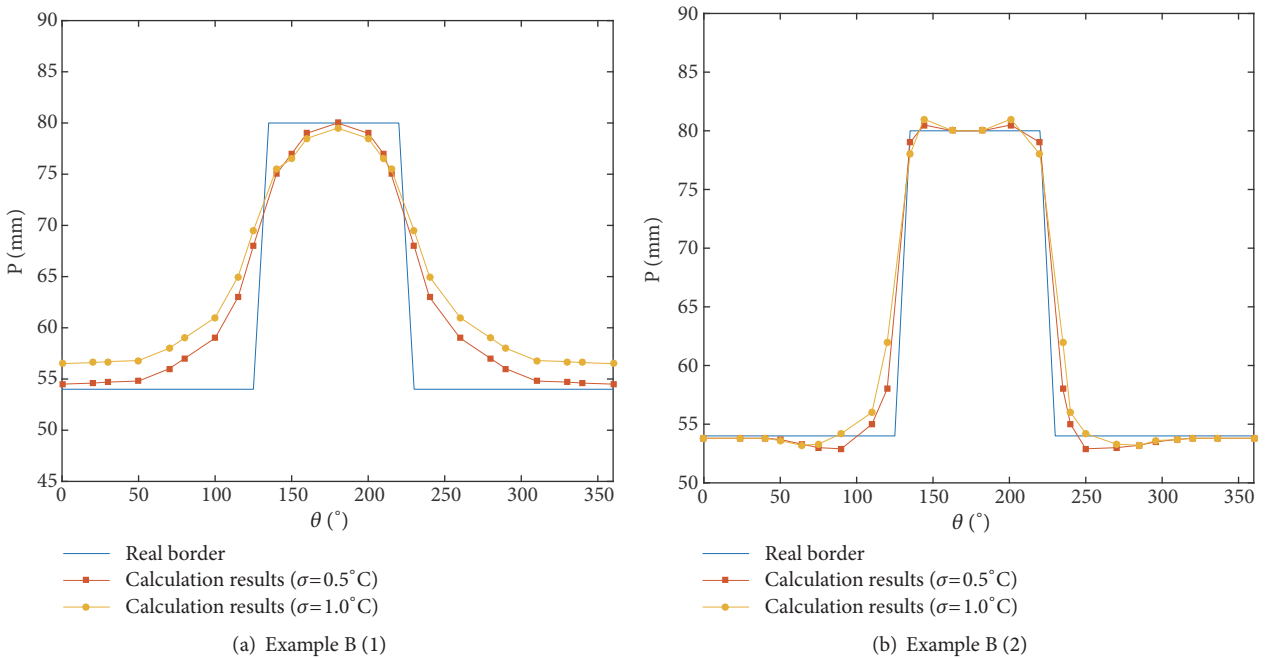

Figure 9: Influence of temperature measurement error on the recognition result concerning the in-wall boundary B.

Figure 14. Influence of temperature measurement error on the average relative error regarding recognition algorithm is shown in Table 3.

Figure 13 shows the influence of the calculation error concerning the heat source intensity on the recognition result, and the average error of the recognition result is within 2.0% when the estimated error of the heat source intensity is ±10%. Thus its influence can be ignored. It can be found from Figure 14 and Table 3 that when the measurement errors are 1.0, 2.0 and 3.0, the average errors are 5.0%, 9.5%, and 12.6%, respectively, indicating that the temperature measurement errors have little influence on the identification results.

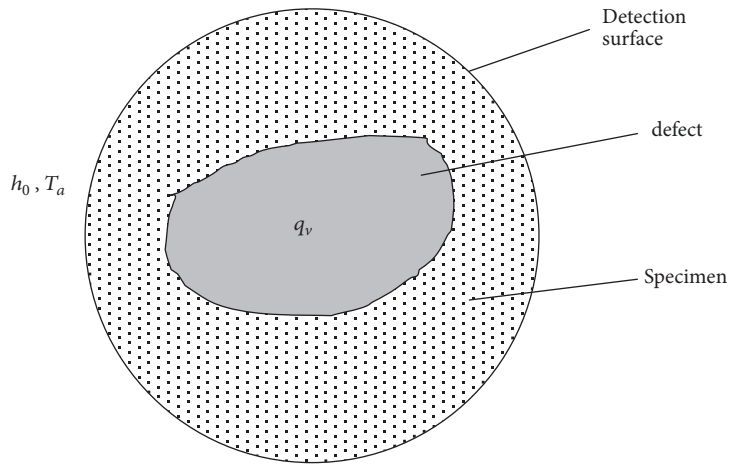

Figure 10: Sketch map of the test piece concerning thermal flaw.

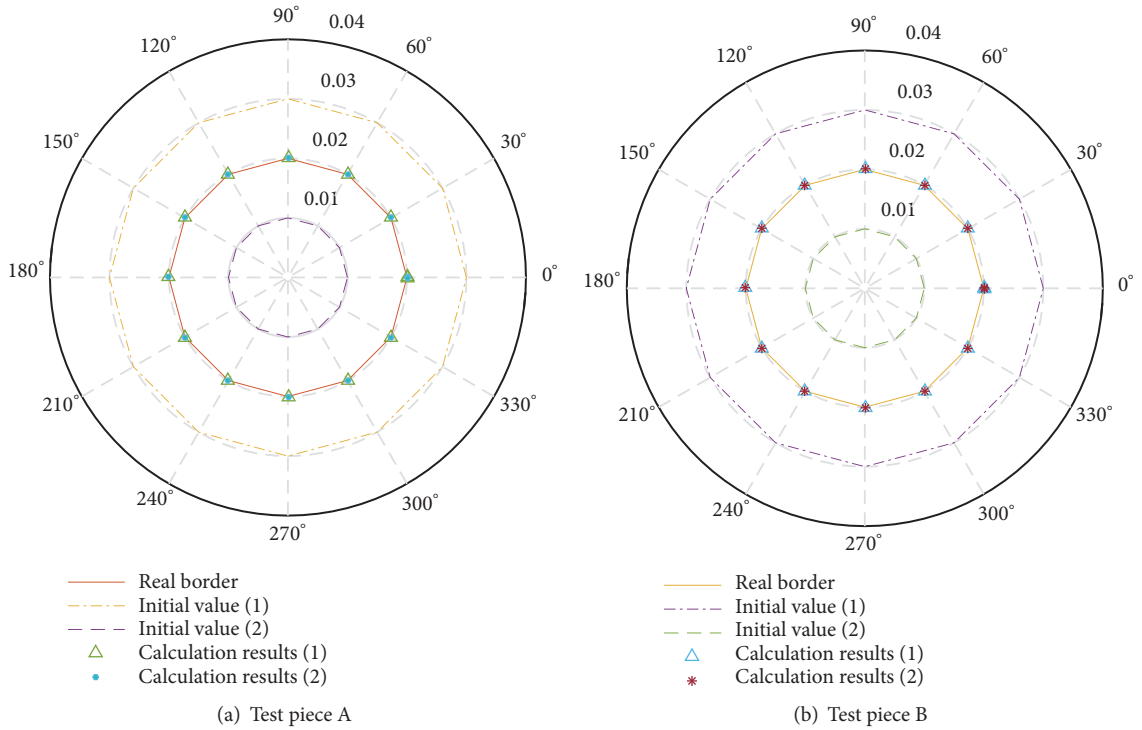

Figure 11: Recognition result of the internal round flaws for two test pieces at different initial values.

6. Conclusions

The direct problem is solved in BEM in this paper, the inverse algorithm based on BEM and CGM is adopted to solve the thermal inverse problems, such as the recognition of boundary shape regarding the pipe in-wall and thermal flaw in test piece. The recognition of test pieces concerning different materials in the shapes such as sinusoidal, step function, or circular shape at the unknown boundary is considered, and the influence of factors such as initial value, temperature measurement error, thermal conductivity, and heating intensity on the precision concerning the inverse solution is discussed. The conclusions are as follows:

(1) The CGM can accurately identify the boundary shape of the inner wall of the pipeline by using the temperature profiler on the outer surface of the pipeline. The initial value has little effect on the recognition results. The smaller the thermal conductivity of the pipeline is, the higher the accuracy of the identification results.

(2) For heating defects, the initial assumption of the defect boundary, the estimation error of the heat source strength, and the measurement error of the testing surface temperature have little influence on the identification results. It is proved that the CGM can accurately identify the boundary contour of the thermal defect.

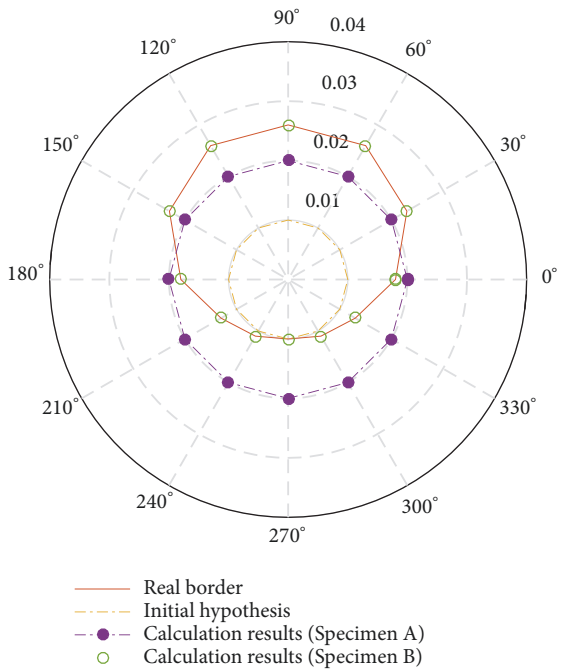

Figure 12: Recognition result concerning flaw boundary shapes regarding two test pieces at the same initial value.

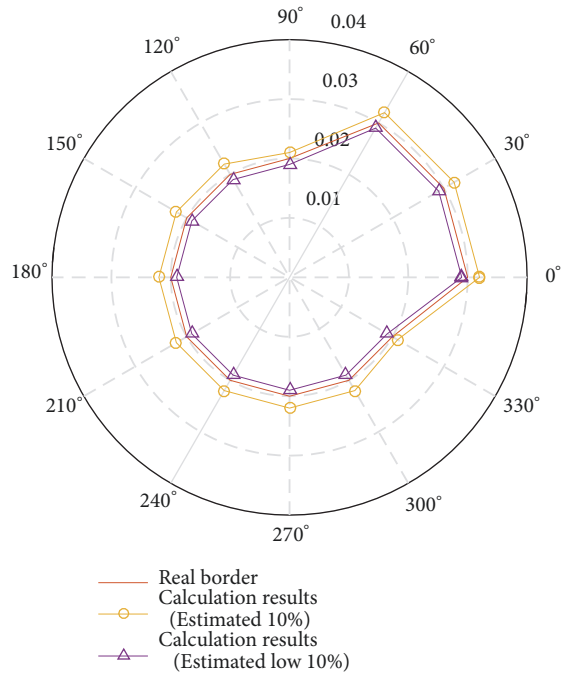

Figure 13: Influence of the calculation error regarding thermal intensity on the recognition result concerning flaws (ε = 2.0).

Table 3: Influence of temperature measurement error on the average relative error regarding recognition algorithm.

Random error	
σ/°C	The average relative error of the results/%
1.0	5.0
2.0	9.5
3.0	12.6

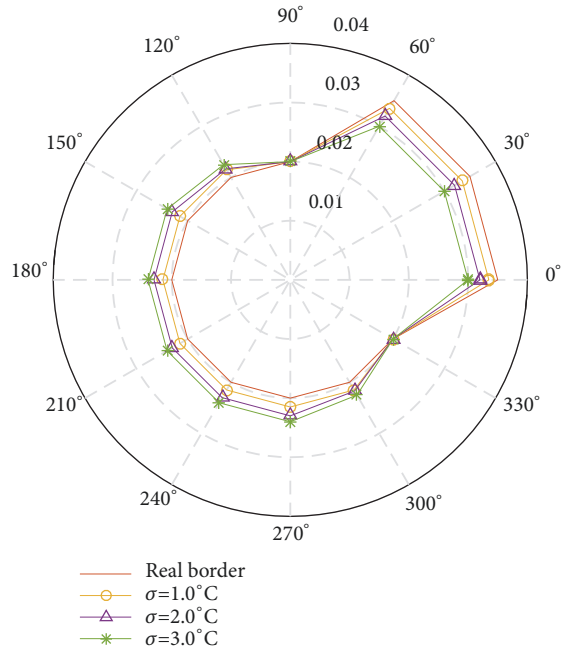

Figure 14: Influence of random temperature measurement error on the recognition result regarding flaws.

Data Availability

The data used to support the findings of this study are available from the corresponding author upon request.

Disclosure

The founding sponsors had no role in the design of the study; in the collection, analyses, or interpretation of data; in the writing of the manuscript; and in the decision to publish the results.

Conflicts of Interest

The authors declare no conflicts of interest.

Acknowledgments

This work was financially supported by the National Key Foundation for Exploring Scientific Instrument of China (2013YQ470767), Tianjin Science and Technology Committee for Science and Technology Development Strategy Research Project (15ZLZLZF00350), Tianjin Science and Technology Commissioner Project (16JCTPJC53000), and the 13th Five-Year Plan (2016-2020) of Science Education Project in Tianjin City (HE1017).

References

[1] S. Wang, H. Jia, X. Sun, and L. Zhang, "Two-Dimensional Steady-State Boundary Shape Inversion of CGM-SPSO Algorithm on Temperature Information," *Advances in Materials Science and Engineering*, vol. 2017, 2017.

[2] S. Wang, L. Zhang, X. Sun, and H. Jia, "Solution to Two-Dimensional Steady Inverse Heat Transfer Problems with Interior Heat Source Based on the Conjugate Gradient Method," *Mathematical Problems in Engineering*, vol. 2017, Article ID 2861342, 9 pages, 2017.

[3] C.-H. Huang and S.-P. Wang, "A three-dimensional inverse heat conduction problem in estimating surface heat flux by conjugate gradient method," *International Journal of Heat and Mass Transfer*, vol. 42, no. 18, pp. 3387–3403, 1999.

[4] C.-H. Huang and C.-W. Chen, "A boundary element-based inverse-problem in estimating transient boundary conditions with conjugate gradient method," *International Journal for Numerical Methods in Engineering*, vol. 42, no. 5, pp. 943–965, 1998.

[5] D. T. W. Lin and C.-Y. Yang, "The estimation of the strength of the heat source in the heat conduction problems," *Applied Mathematical Modelling*, vol. 31, no. 12, pp. 2696–2710, 2007.

[6] H.-K. Liu, L. Yang, and F.-R. Sun, "Estimate method for parameters of asynchronous motor based on inverse heat conduction problem analysis," *Zhongguo Dianji Gongcheng Xuebao/ Proceedings of the Chinese Society of Electrical Engineering*, vol. 26, no. 22, pp. 151–156, 2006.

[7] C.-R. Su and C.-K. Chen, "Geometry estimation of the furnace inner wall by an inverse approach," *International Journal of Heat and Mass Transfer*, vol. 50, no. 19-20, pp. 3767–3773, 2007.

[8] C.-H. Huang, C.-C. Chiang, and S.-K. Chou, "An Inverse Geometry Design Problem in Optimizing Hull Surfaces," *Journal of Ship Research*, vol. 42, no. 2, pp. 79–85, 1998.

[9] P. W. Partridge and L. C. Wrobel, "An inverse geometry problem for the localisation of skin tumours by thermal analysis," *Engineering Analysis with Boundary Elements*, vol. 31, no. 10, pp. 803–811, 2007.

[10] H. Fu, M. K. Ng, and H. Wang, "A divide-and-conquer fast finite difference method for space–time fractional partial differential equation," *Computers & Mathematics with Applications*, 2016.

[11] Z. Zhao, X.-Q. Jin, and Z.-J. Bai, "A geometric nonlinear conjugate gradient method for stochastic inverse eigenvalue problems," *SIAM Journal on Numerical Analysis*, vol. 54, no. 4, pp. 2015–2035, 2016.

[12] M. Feischl, "Adaptive boundary element methods for optimal convergence of point errors," *Numerische Mathematik*, vol. 132, no. 3, pp. 541–567, 2016.

[13] K. Zhou, J. Hou, H. Fu, B. Wei, and Y. Liu, "Estimation of relative permeability curves using an improved Levenberg-Marquardt method with simultaneous perturbation Jacobian approximation," *Journal of Hydrology*, vol. 544, pp. 604–612, 2017.

[14] B. A. Norman and J. C. Bean, "A genetic algorithm methodology for complex scheduling problems," *Naval Research Logistics (NRL)*, vol. 46, no. 2, pp. 199–211, 1999.

[15] M. Ghaedi, A. Ansari, P. A. Nejad, A. Ghaedi, A. Vafaei, and M. H. Habibi, "Artificial neural network and bees algorithm for removal of eosin b using cobalt oxide nanoparticle-activated carbon: Isotherm and kinetics study," *Environmental Progress and Sustainable Energy*, vol. 34, no. 1, pp. 155–168, 2015.

[16] S. Zhang et al., "Optimal Computing Budget Allocation for Particle Swarm Optimization in Stochastic Optimization," *IEEE Transactions on Evolutionary Computation*, vol. 1, no. 1, 2016.

[17] C. Fan, F. Sun, and L. Yang, "An algorithm study on the identification of a pipeline's irregular inner boundary based on thermographic temperature measurement," *Measurement Science and Technology*, vol. 18, no. 7, pp. 2170–2177, 2007.

[18] Y. Chen, T. Yongji, G. Xinaglin et al., "Using inverse problems and genetic algorithms to monitor the thermal erosion of blast furnace hearth," *Journal of Fudan University (Natural Science Edition)*, vol. 45, no. 2, pp. 170–176, 2006.

[19] F. Chunli, F. Sun, L. Yang et al., "Study on a new quantitative the rmographic evaluation method of three-dimensional subsurface defect for electric apparatus," in *Proceedings of the CSEE*, vol. 26, pp. 159–164, 2006.

[20] F. Chunli, S. Fengrui, and L. Yang, "Study on numerical method determining size and position of subsurface defect based on thermographic temperature measurement," *Journal of Thermal Science and Technology*, vol. 4, no. 1, pp. 82–86, 2005.

[21] C.-H. Huang and B.-H. Chao, "An inverse geometry problem in identifying irregular boundary configurations," *International Journal of Heat and Mass Transfer*, vol. 40, no. 9, pp. 2045–2053, 1997.

[22] D. Qinghua and Y. Zhenhan, "Boundary Integral Equation-Boundary Element Method Basic Theory and Some Engineering Applications in Elasticity," *Journal of Solid Mechanics*, p. 1, 1982.

[23] W. Yuanchun, *Boundary Element Method Basics*, Shanghai Jiaotong University Press, Shanghai, 1988.

[24] Y. Shouguang, *Boundary Element Method and Its Engineering Application*, National Defense Industry Press, Beijing, 1995.

[25] L. Bin, *Boundary Element Method for Geometric Inverse Problem of Thermal Conductivity*, Harbin Institute of Technology, 2008.

[26] N. Tian, *Research and Application of Numerical Solution of Inverse Problem for Partial Differential Equation*, Jiangnan University, 2012.